In: Computer Physics
Editors: B.S. Doherty and A.N. Molloy, pp. 315-332
ISBN: 978-1-61324-790-7

Chapter 5

SIMULATION OF COLLISIONLESS PLASMA WITH THE VLASOV METHOD

Takayuki Umeda*
Solar-Terrestrial Environment Laboratory, Nagoya University, Aichi, Japan

Abstract

Numerical schemes for solving the Vlasov-Maxwell system of equations are presented. Our Universe is filled with collisionless plasma, which is a dielectric medium with nonlinear interactions between charged particles and electromagnetic fields. Thus computer simulations play an essential role in studies of such highly nonlinear systems. The full kinetics of collisionless plasma is described by the Vlasov-Maxwell equations. Since the Vlasov equation treats charged particles as position-velocity phase-space distribution functions in hyper dimensions, huge supercomputers and highly-scalable parallel codes are essential. Recently, a new parallel Vlasov-Maxwell solver is developed by adopting a stable but less-dissipative scheme for time integration of conservation laws, which has successfully achieved a high scalability on massively parallel supercomputers with multi-core scalar processors. The new code has applied to 2P3V (two dimensions for position and three dimensions for velocity) problems of cross-scale plasma processes such as magnetic reconnection, Kelvin-Helmholtz instability and the interaction between the solar wind and an asteroid.

PACS 52.65.-y, 52.65.Ff, 52.25.Dg, 52.30.Cv,

Keywords: plasma; electromagnetic wave; conservation law; multi-scale physics

AMS Subject Classification: 82D10, 83C50, 35L65

1. Introduction

No less than 99.9% of the matter in the visible Universe is in the plasma state. The plasma is a gas in which a certain portion of particles are ionized, which is considered to be the “fourth” state of the matter (solid, liquid, gas, and plasma). The Universe is filled with

*E-mail address: umeda@stelab.nagoya-u.ac.jp

plasma particles ejected from the upper atmosphere of stars. The stream of plasma is called the stellar wind, which also carries the intrinsic magnetic field of the stars.

Our solar system is filled with plasma particles ejected from the Sun as the solar wind. Neutral gases in the upper atmosphere of the Earth are ionized by a photoelectric effect due to absorption of energy from sunlight, and the most of these ionized particles are trapped by the intrinsic magnetic field of the Earth. The number density far above the Earth's ionosphere is $\sim 100\mathrm{cm}^{-3}$ or much less, and a typical mean-free path of solar-wind plasma is about 1AU[1]. The number density of plasma particles in space is so low that the system is regarded as collisionless. The word "space plasma" is generally equivalent to collisionless plasma.

The motion of plasma particles is affected by electromagnetic fields due to the electromagnetic Coulomb-Lorentz force. The change in the motion of plasma particles results in an electric current, which modifies the surrounding electromagnetic fields. Thus the plasma behaves as a dielectric medium with strong nonlinear interactions between plasma particles and electromagnetic fields. The computer simulation plays an essential role for studying nonlinear behavior of space plasma. The purpose of this chapter is to give a brief review on the numerical schemes for a first-principle simulation in space plasma based on the Vlasov-Maxwell equations.

2. Basic Equations

There are numerous types of self-consistent computer simulations on space plasma that treat charged particles according to several approximations. The macroscopic (fluid-scale) processes are commonly described by magneto-hydro-dynamic (MHD) or multi-fluid equations, while microscopic (particle-scale) processes are described by the kinetic models, i.e., the Maxwell equations (1) and either the Newton-Lorentz equations (2) or the Vlasov (collisionless Boltzmann) equation (3).

$$\left.\begin{aligned} \nabla \times \mathbf{B} &= \mu_0 \mathbf{J} + \frac{1}{c^2}\frac{\partial \mathbf{E}}{\partial t} \\ \nabla \times \mathbf{E} &= -\frac{\partial \mathbf{B}}{\partial t} \\ \nabla \cdot \mathbf{E} &= \frac{\rho}{\epsilon_0} \\ \nabla \cdot \mathbf{B} &= 0 \end{aligned}\right\} \tag{1}$$

$$\left.\begin{aligned} \frac{\mathrm{d}\mathbf{r}_n}{\mathrm{d}t} &= \mathbf{v}_n \\ \frac{\mathrm{d}\mathbf{v}_n}{\mathrm{d}t} &= \frac{q_n}{m_n}\left[\mathbf{E} + \mathbf{v}_n \times \mathbf{B}\right] \end{aligned}\right\} \tag{2}$$

$$\frac{\partial f_s}{\partial t} + \mathbf{v}\frac{\partial f_s}{\partial \mathbf{r}} + \frac{q_s}{m_s}\left[\mathbf{E} + \mathbf{v} \times \mathbf{B}\right]\frac{\partial f_s}{\partial \mathbf{v}} = 0 \tag{3}$$

where $\mathbf{E}$, $\mathbf{B}$, $\mathbf{J}$, ρ, μ_0, ϵ_0 and c represent the electric field, magnetic field, current density, charge density, magnetic permeability, dielectric constant and light speed, respectively. The quantities $\mathbf{r}$, $\mathbf{v}$, q and m in Eq.(2) are the position, velocity, charge, and mass of the n-th

[1] Astronomical Unit: the distance from the Sun to the Earth. 1AU$\sim$150,000,000km.

particle. The Vlasov equation (3) describes the development of the phase-space distribution functions by the electromagnetic (Coulomb-Lorentz) force $\mathbf{F} = q\left[\mathbf{E} + \mathbf{v} \times \mathbf{B}\right]$, with the collision term in the right hand side set to be zero. The distribution function $f_s(\mathbf{r}, \mathbf{v}, t)$ is defined in position-velocity phase space with the subscript s being the species of singly-charged particles (e.g., $s = i, e$ for ions and electrons, respectively). The Maxwell equations and either the Newton-Lorentz equations or the Vlasov equation are coupled with each other via the current density $\mathbf{J}$ that satisfies the continuity equation for charge

$$\frac{\partial \rho}{\partial t} + \nabla \cdot \mathbf{J} = 0 \tag{4}$$

These kinetic equations are regarded as the "first principle" of collisionless plasma.

The above equations can treat all physical processes in space plasma, from the fluid-scale (macroscopic) dynamics, such as the solar wind, solar flares, and global magnetospheres of stars and planets, to the particle-scale (microscopic) kinetics such as particle acceleration, particle diffusion, and wave-particle interactions. The Newton-Lorentz equation treats the motion of N-particles. This means that the computational load depends on the number of particles (N). The Vlasov equation treats the evolution of phase-space distributions in "hyper" dimensions (higher than four dimensions): three dimensions in configuration space and three dimensions in velocity space for an example.

One may understand that it is not easy to solve macroscopic processes by the first-principle kinetic models, and that fluid models are appropriate for solving the macro scale. The fluid equations are derived by taking the zeroth, first, and second moments of the Vlasov equations (3), where the zeroth, first, and second moments correspond to the conservation laws of the density, momentum, and energy, respectively.

$$\frac{\partial n_s}{\partial t} + \nabla \cdot (n_s \mathbf{u}_s) = 0 \tag{5}$$

$$\frac{\partial}{\partial t}\left(m_s n_s \mathbf{u}_s\right) + \nabla \cdot \left(m_s n_s \mathbf{u}_s \mathbf{u}_s + \mathbf{P}_s\right) - \rho_s \mathbf{E} - \mathbf{J}_s \times \mathbf{B} = 0 \tag{6}$$

$$\frac{\partial}{\partial t}\left(\frac{1}{2} m_s n_s |\mathbf{u}|_s^2 + \frac{3}{2} p_s\right) + \nabla \cdot \left(\frac{1}{2} m_s n_s |\mathbf{u}|_s^2 \mathbf{u}_s + \frac{3}{2} p_s \mathbf{u}_s + \mathbf{P}_s \cdot \mathbf{u}_s + \mathbf{h}_s\right) - \mathbf{E} \cdot \mathbf{J}_s = 0 \tag{7}$$

where $\mathbf{u}$ represents the average velocity, i.e., the flow velocity, $\mathbf{P}_s$ represents the pressure tensor, p_s represents a scalar pressure given by the trace of $\mathbf{P}_s$ ($p_s \equiv \frac{1}{3} \sum_{i=x,y,z} P_{i,i,s}$), and $\mathbf{h}_s$ represents the heat flux density of the s-th fluid. The Magneto-Hydro-Dynamic (MHD) equations are obtained by applying the single-fluid approximation to these equations.

When we consider low-frequency phenomena with a timescale much longer than electron plasma or cyclotron oscillations, the electromagnetic light-mode waves and electron dynamics can be neglected. Then, the displacement current in Eq.(1) becomes negligible, i.e., $\frac{\partial \mathbf{E}}{\partial t} = 0$, which is called the Darwin approximation [1]. In this case, the electric field is derived from the equation of motion for electron fluid.

$$\frac{\partial}{\partial t}\left(m_e n_e \mathbf{u}_e\right) + \nabla \cdot \left(m_e n_e \mathbf{u}_e \mathbf{u}_e\right) = -\nabla \cdot \mathbf{P}_e + \rho_e \mathbf{E} + \mathbf{J}_e \times \mathbf{B} \tag{8}$$

In the low-frequency phenomena, the left hand side in Eq.(8) can be set to be zero ($m_i \gg m_e \to 0$), and the electric field is obtained as

$$\mathbf{E} = -\mathbf{u}_e \times \mathbf{B} + \frac{\nabla \cdot \mathbf{P}_e}{\rho_e} = -\mathbf{u}_i \times \mathbf{B} + \frac{\mathbf{J} \times \mathbf{B}}{\rho_i} - \frac{\nabla \cdot \mathbf{P}_e}{\rho_i} \tag{9}$$

where the total current density is given by $\mathbf{J} = \mathbf{J}_i + \mathbf{J}_e$ and the quasi charge neutrality is assumed ($\rho_e + \rho_i \to 0$). Note that the second term in the right hand side of Eq.(9) ($(\mathbf{J} \times \mathbf{B})/\rho_i$) is called the Hall term. The above equation is used in the Hall-MHD and hybrid models. Note that the hybrid model treat ions particles but electrons as a fluid by Eq.(9), in which only full kinetics of ions are included.

It is noted that the fluid approximations need resistivity, conductivity, adiabatic index, or diffusion coefficients as a closure model of higher-order moments that describes the time development of off-diagonal pressure terms and the heat flux. However, these coefficients are essentially due to first-principle kinetic processes that are eliminated in the framework of the fluid approximations. In this chapter, we especially focus on the first-principle Vlasov-Maxwell model where full kinetics of both ions and electrons are included by solving the Maxwell equations (1) together with the Vlasov equation (3) and the continuity equation for charge (4).

3. Historical Development

Numerical procedures for solving kinetic equations of collisionless plasma have been studied for more than a half century since the advent of the von Neumann-type computers in late 1940's. As described in Sec.2., there are two approaches for solving kinetic equations of collisionless plasma. One is to solve the Newton-Lorentz equations (2), and the other is to solve the Vlasov equation (3). The former one is called the particle-in-cell (PIC) method, because plasma particles are treated as individual charged particles and they freely moves in grid cells of electromagnetic fields. The standard explicit PIC method is a well-developed numerical technique which has numerical procedures and concepts that are quite simple without approximation in the basic laws of collisionless plasma. The PIC method is very powerful and widely used for studying full kinetics in space plasma since 1960's. However, this method has a drawback in numerical noises, because a limitation on the number of particles per cell gives rise to strong numerical thermal fluctuations. There is also a difficulty in load-balancing for massively parallel computers. Since the PIC method uses both Eulerian variables (field variables that depend on both time and space) and Lagrangian variables (particle positions and velocities that depend only on time), the number of particles on each processor element (PE) becomes sometimes nonuniform.

The latter approach is called the Vlasov method, in which spatial and temporal developments of distribution functions defined in the position-velocity phase space are directly solved based on the Vlasov equation (3). The Vlasov method is considered to be an alternative to the PIC method, because this method is free from numerical noises. However, computational load of the Vlasov method is much heavier than that of the PIC method, and therefore the development of numerical schemes for the Vlasov method is much slower than those for the PIC method.

Ideas of standard methods for time integration of the Vlasov equation were established in 1970's. One of standard time-advance methods for Vlasov simulations is the spectral methods [2–5], in which phase-space distribution functions are transformed to spectral components in configuration and velocity spaces by the Fourier or Hermite transformation. Another standard time-advance method is based on a time-advance algorithm called the "splitting scheme" [6, 7]. In 1970's, computer simulations with two dimensions were familiar because the physical size of computer memory was so small (less than hundred MBs). Let us consider a simple 1P1V (one dimension in position and one dimension in velocity) phase space as in 1970's. By neglecting the effect of the magnetic field, the Vlasov-Maxwell equations are reduced as follows.

$$\frac{\partial E_x}{\partial x} = \frac{\rho}{\epsilon_0} \tag{10}$$

$$\frac{\partial f_s}{\partial t} + v_x \frac{\partial f_s}{\partial x} + \frac{q_s}{m_s} E_x \frac{\partial f_s}{\partial v_x} = 0 \tag{11}$$

With the operator splitting, the Vlasov equation (11) is separated into the following two advection equations.

$$\frac{\partial f_s}{\partial t} + v_x \frac{\partial f_s}{\partial x} = 0 \tag{12}$$

$$\frac{\partial f_s}{\partial t} + \frac{q_s}{m_s} E_x \frac{\partial f_s}{\partial v_x} = 0 \tag{13}$$

This means that the formal solutions to the Vlasov equation (11) is approximated by the solutions to the two advection equations [8].

$$f_s\left(x_i, v_{x,j}, t + \Delta t\right) = f_s\left(x_i - v_{x,j}\Delta t, v_{x,j} - \frac{q_s}{m_s} E_{x,i}\Delta t, t\right) \tag{14}$$

$$\sim f_s^*\left(x_i, v_{x,j} - \frac{q_s}{m_s} E_{x,i}\Delta t\right), \quad f_s^*\left(x_i, v_{x,j}\right) = f_s\left(x_i - v_{x,j}\Delta t, v_{x,j}, t\right) \tag{15}$$

Here, the phase-space distribution functions are descritized on a two-dimensional mesh in the $x - v_x$ plane, and the advection velocities v_x and $\frac{q_s}{m_s}E_x$ are functions of v_x and x, respectively. Equation (15) represents a shift of the distribution function in the x direction, and then the distribution function has to be shifted in the v_x direction. One may understand that the general solution to the two-dimensional advection equation (14) is well approximated by Eq.(15) when the advection velocities are constant for all x, v_x, and t. However, this approximation is valid for the Vlasov equation only in a short time scale (Δt), in which the profile of a phase-space distribution function does not move over one cell mesh (Δx and Δv). Note that the splitting scheme for the 1P1V phase space has been extended to hyper-dimensional phase space including the effect of the magnetic field [9, 10]. However, there have not been applications of hyper-dimensional Vlasov-Maxwell solvers to nonlinear plasma physics until 1990's because of the limitation of computer memory.

The idea of the splitting scheme is widely adopted in recent Vlasov solvers because of its simplicity of the algorithms and ease of programming. The time integration of the Vlasov equation is approximated by combinations of the one-dimensional numerical interpolation as seen in Eq.(15). Since the Vlasov solvers in the 20th century adopt the

cubic spline interpolation as the one-dimensional numerical interpolation [6, 7], they are also called semi-Lagrangian Vlasov solvers where the solution can be approximated as a function of time (see e.g., Eqs.(14) and (15)). Recently, this idea is extended to the B-spline interpolation (e.g., Refs. [11, 12]), the CIP (constrained interpolation profile) scheme [13–15], and conservative semi-Lagrangian schemes (e.g., Refs. [16–22]). Although numerical diffusion in conservative semi-Lagrangian schemes is somewhat higher than that in non-conservative semi-Lagrangian schemes, the conservative semi-Lagrangian schemes appear to be more efficient for Vlasov simulations of several classical problems of plasma physics [17, 19, 21, 23]. The inherent conservative property is important in plasma physics, because electromagnetic fields are affected by the current density that satisfies the charge conservation law. In addition, conservative schemes has an advantages in easiness for introducing slope limiters in the reconstruction to ensure specific properties such as positivity and monotonicity [22].

There are not many examples of hyper-dimensional Vlasov-Maxwell simulations for studies of nonlinear plasma physics. 2P2V Vlasov-Maxwell solvers have been applied to the interaction between laser (intense electromagnetic waves) and unmagnetized plasma since 1990's (e.g., Refs. [10, 24]). In recent days, hyper-dimensional (2P2V and 3P2V) Vlasov-Maxwell solvers are applied to magnetically confined plasma, such as tokamak plasma in thermonuclear fusion devices, with the guiding center, drift-kinetic and gyrokinetic approximations (e.g., Refs. [25, 26]). For magnetized plasma, a 1P3V Vlasov-Maxwell solver is applied to wave-particle interactions (e.g., Refs [27]), where the velocity space is taken in the Cylindrical (polar) coordinate [28]. In these previous works, non-conservative semi-Lagrangian schemes were adopted in hyper-dimensional Vlasov-Maxwell solvers in 1990' and early 2000's, while recent hyper-dimensional Vlasov-Maxwell solvers adopt conservative schemes. Note that hyper-dimensional Vlasov-Maxwell solvers based on spectral schemes have also been proposed (e.g., Refs [29]). However, applications of these solvers are limited to linear instability problems. Only recent hyper-dimensional Vlasov-Maxwell solvers with conservative schemes have successfully applied to multi-dimensional problem on nonlinear processes in Geophysics [30–33].

4. Numerical Procedures

4.1. Time-advance Scheme

The Vlasov equation (3) consists of two advection equations with a constant advection velocity and a rotation equation by a centripetal force without diffusion terms. To simplify the numerical time-integration of the Vlasov equation, we adopt an operator splitting technique for magnetized plasma [6, 10]. We have developed a modified version of the operator splitting, where the Vlasov equation splits into the following three equations [34],

$$\frac{\partial f_s}{\partial t} + \mathbf{v}\frac{\partial f_s}{\partial \mathbf{r}} = 0 \tag{16}$$

$$\frac{\partial f_s}{\partial t} + \frac{q_s}{m_s}\mathbf{E}\frac{\partial f_s}{\partial \mathbf{v}} = 0 \tag{17}$$

$$\frac{\partial f_s}{\partial t} + \frac{q_s}{m_s}\left[\mathbf{v}\times\mathbf{B}\right]\frac{\partial f_s}{\partial \mathbf{v}} = 0 \tag{18}$$

Equations (16) and (17) are scalar (linear) advection equations in which $\mathbf{v}$ and $\mathbf{E}$ are independent of $\mathbf{r}$ and $\mathbf{v}$, respectively. We have developed a multidimensional conservative semi-Lagrangian scheme for solving these two advection equations [34], which is briefly reviewed in Subsection 4.2. Note that it is essential to use conservative schemes for satisfying the continuity equation for charge in the full electromagnetic method. With the multidimensional conservative semi-Lagrangian scheme, the solution to the advection equation in the configuration space (16) is given by

$$f_{i,j,k}^{t+\Delta t} \leftarrow f_{i,j,k}^{t} + \frac{\Delta t}{\Delta x}\left[U_{x,i+\frac{1}{2},j,k} - U_{x,i-\frac{1}{2},j,k}\right] + \frac{\Delta t}{\Delta y}\left[U_{y,i,j+\frac{1}{2},k} - U_{y,i,j-\frac{1}{2},k}\right] + \frac{\Delta t}{\Delta z}\left[U_{z,i,j,k+\frac{1}{2}} - U_{z,i,j,k-\frac{1}{2}}\right] \tag{19}$$

where $\mathbf{U} \equiv (U_x, U_y, U_z)$ represent numerical flux in the configuration space, and the subscript s is omitted. One can find that the above equation exactly satisfies the continuity equation for charge (4) with

$$\rho = \sum_s q_s \int f_s \mathrm{d}\mathbf{v} \tag{20}$$

$$\mathbf{J} = \sum_s q_s \int \mathbf{U}_s \mathrm{d}\mathbf{v} \tag{21}$$

In the present study, we adopt a positive, non-oscillatory and conservative scheme [21] for stable time-integration of advection equations, which is briefly reviewed in Subsection 4.3. Equation (18), by contrast, is a multi-dimensional rotation equation which follows a circular motion of a profile at constant angular speed by a centripetal force. For stable rotation of the profile on the Cartesian grid system, the "back-substitution" technique [35] is applied. In addition, Maxwell's equations are solved by the implicit Finite Difference Time Domain (FDTD) method on the Yee grid system [36], which is free from the Courant condition for electromagnetic light mode waves.

The Maxwell-Vlasov system is advanced by using the following sequences [34], which is consistent with the second-order leap-frog time-integration algorithm used in particle-in-cell simulations.

1. Shift phase-space distribution functions in the configuration space with the full time step Δt by using the multidimensional conservative scheme [34].

$$f_s^* (\mathbf{r}, \mathbf{v}) \leftarrow f_s^t (\mathbf{r} - \mathbf{v}\Delta t, \mathbf{v}) \tag{22}$$

2. Compute the current density by integrating the numerical flux $\mathbf{U}$ over the velocity $\mathbf{v}$ as Eq.(21).

3. Advance electromagnetic fields from t to $t + \Delta t$ by solving Maxwell's equations with the implicit FDTD method.

4. Shift phase-space distribution functions in the velocity space by an electric force with the half time step $\Delta t/2$ by using the multidimensional conservative scheme [34].

$$f_s^{**} (\mathbf{r}, \mathbf{v}) \leftarrow f_s^* \left(\mathbf{r}, \mathbf{v} - \frac{q_s}{m_s}\mathbf{E}^{t+\Delta t}\frac{\Delta t}{2}\right) \tag{23}$$

5. Rotate phase-space distribution functions in the velocity space by a magnetic force with the full time step Δt by using the back-substitution scheme [35].

$$f_s^{***}(\mathbf{r},\mathbf{v}) \leftarrow f_s^{**}(\mathbf{r},\mathbf{v}^*) \tag{24}$$

where

$$\mathbf{v}^* = \mathbf{v} - \frac{q_s}{m_s}\frac{\Delta t}{1+\left[\frac{q_s\Delta t}{2m_s}|\mathbf{B}^{t+\Delta t}|\right]^2}\left\{\left[\mathbf{v}\times\mathbf{B}^{t+\Delta t}\right] + \frac{q_s\Delta t}{2m_s}\left[\mathbf{v}\times\mathbf{B}^{t+\Delta t}\times\mathbf{B}^{t+\Delta t}\right]\right\}$$

6. Shift phase-space distribution functions in the velocity space by an electric force with the half time step $\Delta t/2$ by using the multidimensional conservative scheme [34].

$$f_s^{t+\Delta t}(\mathbf{r},\mathbf{v}) \leftarrow f_s^{***}\left(\mathbf{r},\mathbf{v}-\frac{q_s}{m_s}\mathbf{E}^{t+\Delta t}\frac{\Delta t}{2}\right) \tag{25}$$

The detailed descriptions of the numerical schemes are provided in Refs. [21, 34, 35].

In the present Vlasov code, there is a numerical constraint on the Courant condition for rotation in velocity space by magnetic fields. For stable rotation of distribution functions with the back-substitution scheme on the Cartesian grid system, we need to choose the timestep Δt such that

$$\Delta v_e > \frac{q_e}{m_e}|\mathbf{v}_{\max,e}|B_0\Delta t = \omega_{ce}|\mathbf{v}_{\max,e}|\Delta t \tag{26}$$

where B_0 represents an ambient magnetic field. This means that the timestep Δt must be taken to be small for strongly magnetized plasma.

4.2. Multi-dimensional Conservative Scheme

Let us consider that a numerical solution to Eq.(22) takes the following conservative form (see also Eq.(19)),

$$\begin{aligned} f_s^*(x_i,y_j,z_k,v_{x,l},v_{y,m},v_{z,n}) &= f_s^t(x_i,y_j,z_k,v_{x,l},v_{y,m},v_{z,n}) \\ -\frac{\Delta t}{\Delta x}\left[U_{x,s}\left(x_{i+\frac{1}{2}},y_j,z_k,v_{x,l},v_{y,m},v_{z,n}\right) - U_{x,s}\left(x_{i-\frac{1}{2}},y_j,z_k,v_{x,l},v_{y,m},v_{z,n}\right)\right] \\ -\frac{\Delta t}{\Delta y}\left[U_{y,s}\left(x_i,y_{j+\frac{1}{2}},z_k,v_{x,l},v_{y,m},v_{z,n}\right) - U_{y,s}\left(x_i,y_{j-\frac{1}{2}},z_k,v_{x,l},v_{y,m},v_{z,n}\right)\right] \\ -\frac{\Delta t}{\Delta z}\left[U_{z,s}\left(x_i,y_j,z_{k+\frac{1}{2}},v_{x,l},v_{y,m},v_{z,n}\right) - U_{z,s}\left(x_i,y_j,z_{k-\frac{1}{2}},v_{x,l},v_{y,m},v_{z,n}\right)\right] \end{aligned} \tag{27}$$

where U_x, U_y and U_z are numerical fluxes in the x, y and z directions, respectively. The subscripts i, j, k, l, m and n represent the grid numbers. Then, the continuity equation for charge (4) is automatically satisfied.

Although there is an arbitrary solution for the multi-dimensional numerical flux in Eq.(27), we approximate the numerical flux by using one-dimensional numerical flux in x,

y and z directions: $U^{1D}_{x,s}\left(x_{i+\frac{\sigma_i}{2}}, y_j, z_k\right)$, $U^{1D}_{y,s}\left(x_i, y_{j+\frac{\sigma_j}{2}}, z_k\right)$ and $U^{1D}_{z,s}\left(x_i, y_j, z_{k+\frac{\sigma_k}{2}}\right)$.

$$\left.\begin{aligned}
U_{x,s}\left(x_{i+\frac{\sigma_i}{2}}, y_{j+\sigma_j}, z_{k+\sigma_k}\right) &= \sigma_i \frac{\Delta t^2}{\Delta y \Delta z} \frac{U^{1D}_{x,s} U^{1D}_{y,s} U^{1D}_{z,s}}{3\left[f^t_s(x_i, y_j, z_k)\right]^2} \\
U_{x,s}\left(x_{i+\frac{\sigma_i}{2}}, y_{j+\sigma_j}, z_k\right) &= \sigma_i \frac{\Delta t}{\Delta y} \frac{U^{1D}_{x,s} U^{1D}_{y,s}}{2 f^t_s(x_i, y_j, z_k)} - U_{x,s}\left(x_{i+\frac{\sigma_i}{2}}, y_{j+\sigma_j}, z_{k+\sigma_k}\right) \\
U_{x,s}\left(x_{i+\frac{\sigma_i}{2}}, y_j, z_{k+\sigma_k}\right) &= \sigma_i \frac{\Delta t}{\Delta z} \frac{U^{1D}_{x,s} U^{1D}_{z,s}}{2 f^t_s(x_i, y_j, z_k)} - U_{x,s}\left(x_{i+\frac{\sigma_i}{2}}, y_{j+\sigma_j}, z_{k+\sigma_k}\right) \\
U_{x,s}\left(x_{i+\frac{\sigma_i}{2}}, y_j, z_k\right) &= U^{1D}_{x,s} - U_{x,s}\left(x_{i+\frac{\sigma_i}{2}}, y_{j+\sigma_j}, z_k\right) \\
&\quad - U_{x,s}\left(x_{i+\frac{\sigma_i}{2}}, y_j, z_{k+\sigma_k}\right) - U_{x,s}\left(x_{i+\frac{\sigma_i}{2}}, y_{j+\sigma_j}, z_{k+\sigma_k}\right)
\end{aligned}\right\} \tag{28}$$

$$\left.\begin{aligned}
U_{y,s}\left(x_{i+\sigma_i}, y_{j+\frac{\sigma_j}{2}}, z_{k+\sigma_k}\right) &= \sigma_j \frac{\Delta t^2}{\Delta z \Delta x} \frac{U^{1D}_{x,s} U^{1D}_{y,s} U^{1D}_{z,s}}{3\left[f^t_s(x_i, y_j, z_k)\right]^2} \\
U_{y,s}\left(x_i, y_{j+\frac{\sigma_j}{2}}, z_{k+\sigma_k}\right) &= \sigma_j \frac{\Delta t}{\Delta z} \frac{U^{1D}_{y,s} U^{1D}_{z,s}}{2 f^t_s(x_i, y_j, z_k)} - U_{y,s}\left(x_{i+\sigma_i}, y_{j+\frac{\sigma_j}{2}}, z_{k+\sigma_k}\right) \\
U_{y,s}\left(x_{i+\sigma_i}, y_{j+\frac{\sigma_j}{2}}, z_k\right) &= \sigma_j \frac{\Delta t}{\Delta x} \frac{U^{1D}_{x,s} U^{1D}_{y,s}}{2 f^t_s(x_i, y_j, z_k)} - U_{y,s}\left(x_{i+\sigma_i}, y_{j+\frac{\sigma_j}{2}}, z_{k+\sigma_k}\right) \\
U_{y,s}\left(x_i, y_{j+\frac{\sigma_j}{2}}, z_k\right) &= U^{1D}_{y,s} - U_{y,s}\left(x_i, y_{j+\frac{\sigma_j}{2}}, z_{k+\sigma_k}\right) \\
&\quad - U_{y,s}\left(x_{i+\sigma_i}, y_{j+\frac{\sigma_j}{2}}, z_k\right) - U_{y,s}\left(x_{i+\sigma_i}, y_{j+\frac{\sigma_j}{2}}, z_{k+\sigma_k}\right)
\end{aligned}\right\} \tag{29}$$

$$\left.\begin{aligned}
U_{z,s}\left(x_{i+\sigma_i}, y_{j+\sigma_j}, z_{k+\frac{\sigma_k}{2}}\right) &= \sigma_k \frac{\Delta t^2}{\Delta x \Delta y} \frac{U^{1D}_{x,s} U^{1D}_{y,s} U^{1D}_{z,s}}{3\left[f^t_s(x_i, y_j, z_k)\right]^2} \\
U_{z,s}\left(x_i, y_{j+\sigma_j}, z_{k+\frac{\sigma_k}{2}}\right) &= \sigma_k \frac{\Delta t}{\Delta y} \frac{U^{1D}_{y,s} U^{1D}_{z,s}}{2 f^t_s(x_i, y_j, z_k)} - U_{z,s}\left(x_{i+\sigma_i}, y_{j+\sigma_j}, z_{k+\frac{\sigma_k}{2}}\right) \\
U_{z,s}\left(x_{i+\sigma_i}, y_j, z_{k+\frac{\sigma_k}{2}}\right) &= \sigma_k \frac{\Delta t}{\Delta x} \frac{U^{1D}_{z,s} U^{1D}_{x,s}}{2 f^t_s(x_i, y_j, z_k)} - U_{z,s}\left(x_{i+\sigma_i}, y_{j+\sigma_j}, z_{k+\frac{\sigma_k}{2}}\right) \\
U_{z,s}\left(x_i, y_j, z_{k+\frac{\sigma_k}{2}}\right) &= U^{1D}_{z,s} - U_{z,s}\left(x_i, y_{j+\sigma_j}, z_{k+\frac{\sigma_k}{2}}\right) \\
&\quad - U_{z,s}\left(x_{i+\sigma_i}, y_j, z_{k+\frac{\sigma_k}{2}}\right) - U_{z,s}\left(x_{i+\sigma_i}, y_{j+\sigma_j}, z_{k+\frac{\sigma_k}{2}}\right)
\end{aligned}\right\} \tag{30}$$

where $\sigma_i = \mathrm{sign}\left(v_{x,l}\right)$, $\sigma_j = \mathrm{sign}\left(v_{y,m}\right)$ and $\sigma_k = \mathrm{sign}\left(v_{z,n}\right)$. Note that $v_{x,l}$, $v_{y,m}$ and $v_{z,n}$ are omitted for simplicity. Here the one-dimensional numerical flux U^{1D} is computed by using a set of one-dimensional data. For an example, a numerical flux in the x direction, $U^{1D}_{x,s}\left(x_{i+\frac{\sigma_i}{2}}, y_j, z_k\right)$, is obtained as a function of $f(x_i, y_j, z_k)$, $f(x_{i-1}, y_j, z_k)$, $f(x_{i+1}, y_j, z_k)$, $f(x_{i-2}, y_j, z_k)$, $f(x_{i+2}, y_j, z_k)$, $\cdots$. The detailed derivation is given in Ref. [34].

4.3. One-dimensional Conservative Semi-Lagrangian Scheme

We can use an arbitrary conservative scheme to compute the one-dimensional numerical flux U^{1D}. In the present study, we use the positive and non-oscillatory scheme [21]. Let us

consider numerical solutions to the one-dimensional advection equation

$$\frac{\partial f}{\partial t} + v\frac{\partial f}{\partial x} = 0. \tag{31}$$

The general solution of Eq.(31) is obtained as

$$f(t+\Delta t, i\Delta x) = f(t, i\Delta x - v\Delta t) \tag{32}$$

and a numerical solution with the 3rd-degree upwind-biased Lagrange polynomial interpolation is obtained as

$$\begin{aligned} f(x) = f_i + \frac{x-i\Delta x}{\Delta x}(f_i - f_{i-1}) \\ +\frac{x-i\Delta x}{\Delta x}\left(1+\frac{x-i\Delta x}{\Delta x}\right)\left(2+\frac{x-i\Delta x}{\Delta x}\right)\frac{f_{i-1}-2f_i+f_{i+1}}{6} \\ +\frac{x-i\Delta x}{\Delta x}\left(1+\frac{x-i\Delta x}{\Delta x}\right)\left(1-\frac{x-i\Delta x}{\Delta x}\right)\frac{f_{i-2}-2f_{i-1}+f_i}{6} \end{aligned} \tag{33}$$

The conservative form of the above equation is

$$\begin{aligned} U_{i+\frac{1}{2}}(\nu) &= \nu f_i + \nu(1-\nu)(2-\nu)\frac{f_{i+1}-f_i}{6} \\ &\quad +\nu(1-\nu)(1+\nu)\frac{f_i - f_{i-1}}{6} \end{aligned} \tag{34}$$

where $\nu \equiv (i\Delta x - x)/\Delta x$ with

$$f_i^{t+\Delta t} = f_i^t + U_{i-\frac{1}{2}}(\nu) - U_{i+\frac{1}{2}}(\nu) \tag{35}$$

We introduce a flux limiter in Eq.(34) to suppress the numerical oscillation (e.g., Ref. [16]),

$$\begin{aligned} U_{i+\frac{1}{2}}(\nu) &= \nu f_i + \nu(1-\nu)(2-\nu)\frac{L_i^{(+)}}{6} \\ &\quad +\nu(1-\nu)(1+\nu)\frac{L_i^{(-)}}{6} \end{aligned} \tag{36}$$

where

$$\begin{aligned} L_i^{(+)} &= \begin{cases} \min[2(f_i - f_{min}), (f_{i+1}-f_i)] & \text{if } f_{i+1} \geq f_i \\ \max[2(f_i - f_{max}), (f_{i+1}-f_i)] & \text{if } f_{i+1} < f_i \end{cases} \\ L_i^{(-)} &= \begin{cases} \min[2(f_{max} - f_i), (f_i - f_{i-1})] & \text{if } f_i \geq f_{i-1} \\ \max[2(f_{min} - f_i), (f_i - f_{i-1})] & \text{if } f_i < f_{i-1} \end{cases} \end{aligned}$$

with

$$\begin{aligned} f_{max} &= \max[f_{max1}, f_{max2}] \\ f_{min} &= \max[0, \min[f_{min1}, f_{min2}]] \end{aligned}$$

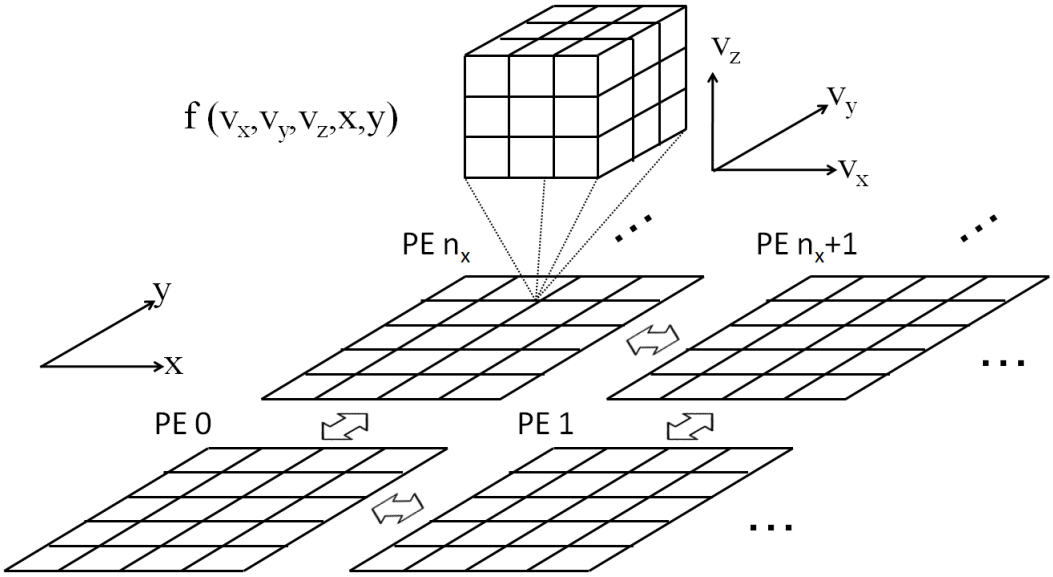

Figure 1. Schematic illustration on the domain decomposition of the 2P3V Vlasov solver.

and

$$f_{max1}=\max\left[\max[f_{i-1},f_i],\min[2f_{i-1}-f_{i-2},2f_i-f_{i+1}]\right]$$
$$f_{max2}=\max\left[\max[f_{i+1},f_i],\min[2f_{i+1}-f_{i+2},2f_i-f_{i-1}]\right]$$
$$f_{min1}=\min\left[\min[f_{i-1},f_i],\max[2f_{i-1}-f_{i-2},2f_i-f_{i+1}]\right]$$
$$f_{min2}=\min\left[\min[f_{i+1},f_i],\max[2f_{i+1}-f_{i+2},2f_i-f_{i-1}]\right]$$

The detailed derivation is given in Ref. [21]. One can see than the present conservative scheme needs five grid points ($f_{i+2}, f_{i+1}, f_i, f_{i-1}, f_{i-2}$) to detect local extrema for computing the numerical flux (and six grid points are needed for interpolation). Note that the conservative scheme based on the third-degree polynomial is now extended to the fourth- and fifth-degree polynomials [37].

4.4. Parallel Implementation

The velocity distribution function has both configuration-space and velocity-space dimensions, and is defined as a hyper-dimensional array, as schematically illustrated in Figure 1. Thus we adopt the "domain decomposition" only in configuration space, where the distribution functions f and electromagnetic fields E_x, E_y, E_z, B_x, B_y, and B_z are decomposed over the configuration-space dimensions (see Figure 1). This involves the exchange of ghost values for the distribution function and electromagnetic field data along each PE boundary. Note that there is additional communication overhead in parallelizing over the velocity-space dimensions since a reduction operation is required to compute the charge and current densities (the zeroth and first moments) at a given point in configuration space as seen in Eqs.(20) and (21). However, the code allows thread parallelization over the velocity-space dimensions via OpenMP.

As seen in Sec.4.1., the Vlasov-Maxwell solver consists of three procedures:

(a) Shifting distribution function in configuration space.

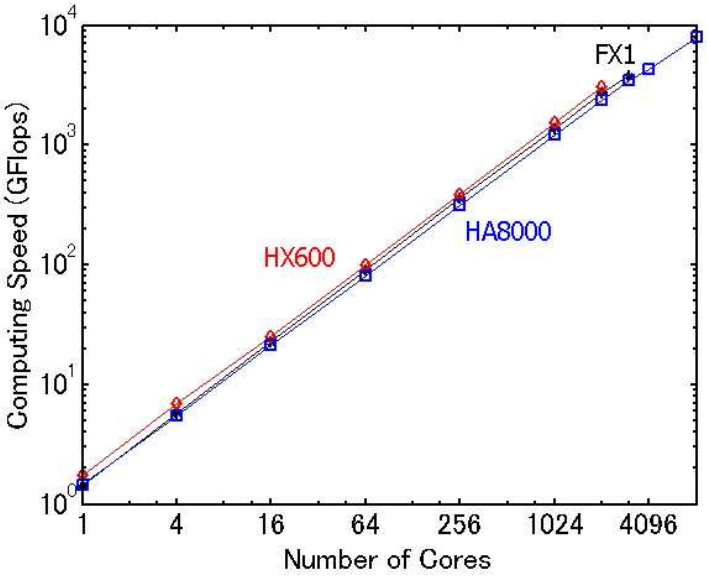

Figure 2. Computational speed of the 2P3V Vlasov solver as a function of the number of cores on various scalar-type supercomputers: Hitach HA8000 system (T2K) at University of Tokyo, Fujitsu FX1 and HX600 systems at Nagoya University.

(b) Shifting distribution function in velocity space.

(c) Updating electromagnetic fields.

Communications between PEs are required at the end of each procedure in order to exchange the ghost values at boundaries. The positive, non-oscillatory and conservative scheme [21] uses six grid points for numerical interpolation (see also Subsec.4.3.), and three ghost grids are exchanged by using the "`Mpi_Sendrecv()`" subroutine in the standard message passing interface (MPI) library for simplicity and portability. The electromagnetic field solver (c) needs additional communications because the convergence check is required in the implicit FDTD method. The "`Mpi_Allreduce()`" subroutine is called on each iteration for the field solver. As shown in Figure 2, the present parallel Vlasov-Maxwell solver achieved a high scalability on various scalar-type supercomputers in Japan.

5. Applications

5.1. Magnetic Reconnection

We adopt the similar initial condition to the Geospace Environment Modeling (GEM) reconnection challenge [38]. There is a Harris-type sheet equilibrium in the $x-y$ plane. We use $N_x \times N_y = 320 \times 160$ grid cells for configuration space, and $N_{v_x} \times N_{v_y} \times N_{v_z} = 40 \times 40 \times 40$ grid cells for velocity space. Thus the simulation domain is taken in the 5D phase space. The half thickness of the current sheet is chosen to be $l = 0.5d_{i0}$, where d_{i0} is the initial ion inertial length ($d_{i0} = c/\omega_{pi0}$) at the center of the current sheet. The ion

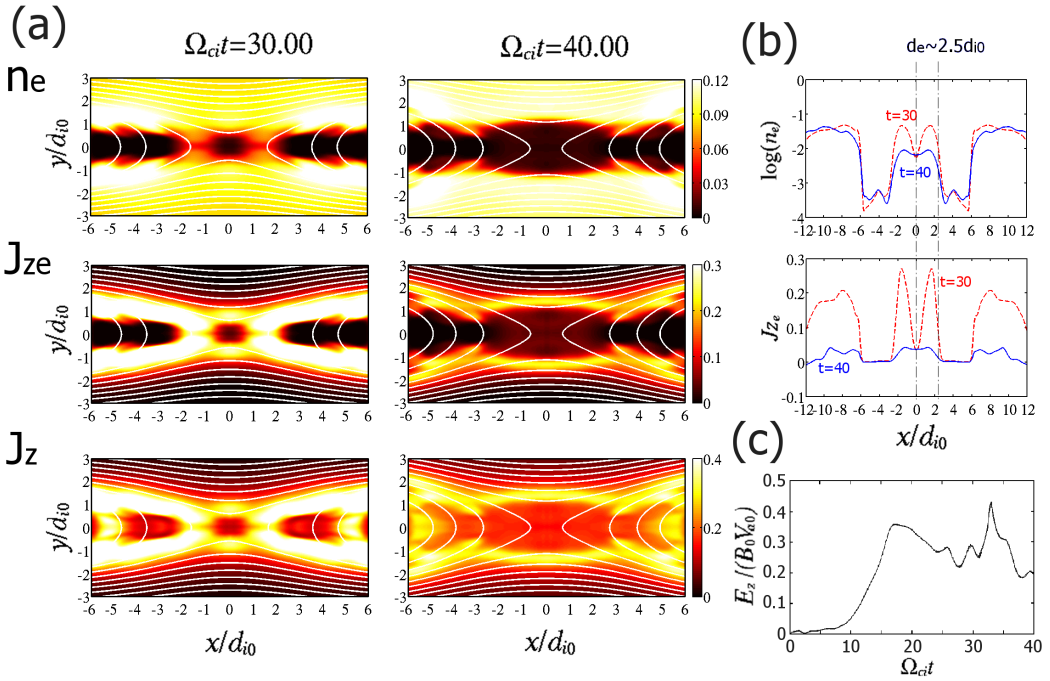

Figure 3. (a) Spatial profiles of the electron number density n_e, the out-of-plane electron current density J_{ze}, and the out-of-plane total current density J_z at $\Omega_{ci}t = 30$ and 40. (b) Cross-section of n_e and J_{ze} at $t = 30, 40$ and $y = 0$. (c) Time history of the reconnection rate.

cyclotron frequency is set as $\omega_{ci}/\omega_{pi} = 0.04$, and the speed of light is set as $c/v_{ti} = 100.0$. For computational efficiency we adopt a very small number of the ion-to-electron mass ratio, $m_i/m_e = 25$. The ion-to-electron temperature ratio is chosen to be $T_i/T_e = 7$. The grid spacing is set as $\Delta = 4.0v_{ti}/\omega_{pi} (= 0.04d_{i0} = 0.2d_{e0})$. Detailed descriptions on the initial setup for the Vlasov simulation are given in Ref. [31]. The boundary conditions are symmetric at the inner boundaries and open at the outer boundaries. That is, we adopt the one quarter model with the symmetry constraints.

Figure 3 shows the nonlinear development of magnetic reconnection. One can see from Figure 3c that the reconnection rate saturates at $\Omega_{ci}t = 18$ but keeps a high value due to the open boundary condition. The spatial profiles of the total current density at $\Omega_{ci}t = 30$ and 40 (Figure 3a) show that the current sheet around the X-point has multiple structures. It is clearly shown that the multiple structures of the current sheet is dominated by electrons, suggesting the existence of multiple electron diffusion regions (e.g., Refs. [39, 40]). Figure 3b shows the cross-section of the electron number density and the out-of-plane electron current density at $t = 30, 40$ and $y = 0$. It is found that the electron number density around the X-point decreases to $\sim 10^{-2} n_{e0}$. Note that the Vlasov method would have an advantage in handling such a low-density region because of its noiselessness. In such a low-density region, the electron inertial length becomes comparable to the ion inertial length, and the spatial scale of the inner electron diffusion region is determined by the local electron inertial length. Note that the ion-to-electron mass ratio in the present simulation is very small, and

therefore it is not easy to separate ion and electron scales. However, this result suggests influence of electron-scale processes on magnetic reconnection.

5.2. Kelvin-Helmholtz Instability

We adopt the same initial condition as the previous works (e.g., Refs. [31, 41]). There are low-density and high-density regions directed in the negative and positive x directions, respectively, which are sheared in the y direction. We use $N_x \times N_y = 512 \times 960$ grid cells for configuration space, and $N_{v_x} \times N_{v_y} = 80 \times 80$ grid cells for velocity space. Thus the simulation domain is taken in the 4D phase space. The half thickness of the shear layer is chosen to be $l = 4.0r_i$ ($r_i = v_{ti}/\omega_{ci}$). The velocity shear is chosen to be $u_0 = \sqrt{V_A^2 + V_S^2} = 7.28v_{ti}$, with the Alfven velocity $V_A = 7.0v_{ti}$ and the ion sound velocity $V_S = 2.0v_{ti}$. A number density ratio of low-density to high-density regions is set as 0.1. The ion cyclotron frequency is set as $\omega_{ci}/\omega_{pi} = 0.0875$, and the speed of light is set as $c/v_{ti} = 80.0$. For computational efficiency we adopt a very small number of the ion-to-electron mass ratio, $m_i/m_e = 16$. The ion-to-electron temperature ratio is chosen to be $T_i/T_e = 1$. The grid spacing is set as $\Delta = 2.0v_{ti}/\omega_{pi} (= 0.175r_i = 0.7r_e)$. The boundary conditions are periodic in the x direction and open in the y direction.

In Figure 4, we show spatial profiles of the total charge density. At $t = 100$ one large vortex is formed by the primary K-H instability, and at $t = 120$ several small vortices are formed by the secondary Rayleigh-Taylor instability [41]. We see that the charge separation in the primary vortex takes place on the spatial scale of the initial half thickness l, while the charge separation in the secondary vortices takes place on the spatial scale of ion cyclotron radius r_i. In Figure 4b, we plot a cross-section of the total charge density at $y/l = -6.7$ and $t = 140$. Note that the distance in Figure 4b is normalized by two different quantities, i.e., l (top) and r_i (bottom). It is found that the spatial scale of small vortices at $y/l = -6.7$ is $\sim 5r_i$ and that the charge separation takes place on the spatial scale smaller than r_i ($\sim 2r_e$). Note that the ion-to-electron mass ratio in the present simulation is very small, and therefore it is not easy to completely separate ion and electron scales. However, this result suggests existence of strong in-plane electrostatic fields on the spatial scale of electron cyclotron radius.

5.3. Interaction between Solar Wind and a Dielectric Body

We adopt the same initial and boundary condition as the previous work [33]. There exists an insulative sphere at $(x, y) = (0, 0)$, in which the charge accumulates at the surface. The system size of the simulation box is taken for $-10R_S \le L_x \le 30R_S$ and $-10R_S \le L_y \le 10R_S$, where R_S is the radius of the object. We use $N_x \times N_y = 400 \times 200$ grid cells for configuration space, and $N_{v_x} \times N_{v_y} \times N_{v_z} = 40 \times 40 \times 40$ grid cells for velocity space. Thus the simulation domain is taken in the 5D phase space. The solar wind velocity is set as $V_s = 12V_{ti}$, and the plasma beta in the solar wind is set as $\beta_i = \beta_e = 0.5$. The magnitude of the interplanetary magnetic field (IMF) is given such that $\omega_{ci}/\omega_{pi} = 0.01$. The radius of the body is set as $R_S = r_i = 10\Delta$. Electrons are assumed to be much heavier than the reality with the mass ratio $m_i/m_e = 100$, and the ions and electrons have the same temperature ($T_i/T_e = 1.0$). The IMF is taken in the out-of-plane (z) direction so that the

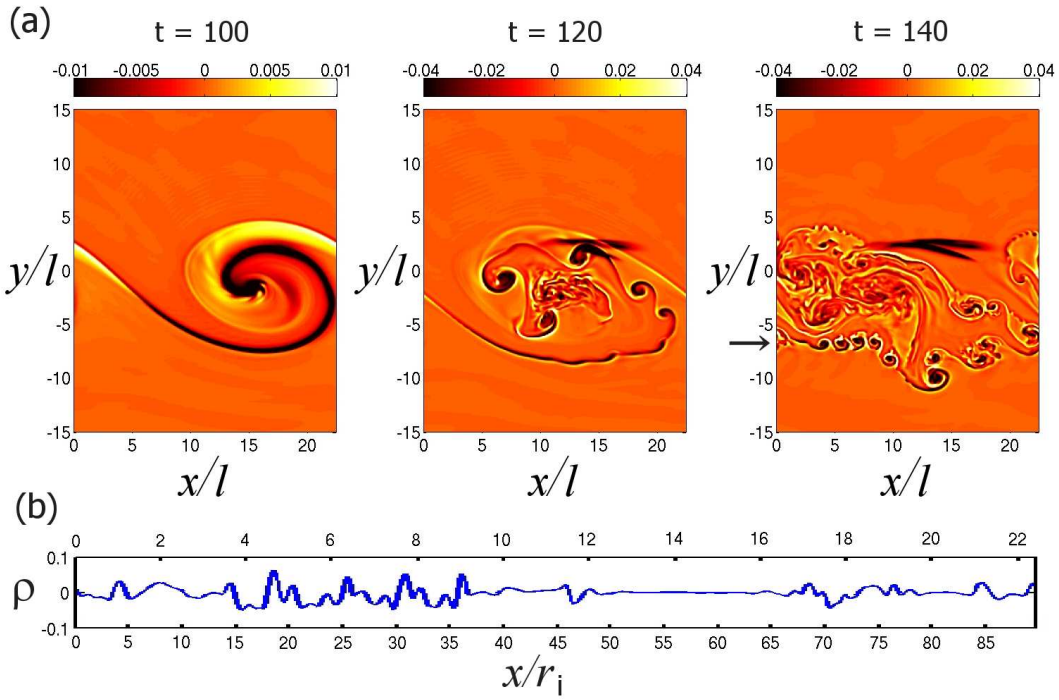

Figure 4. (a) Spatial profiles of the total charge density at different times. (b) Cross-section of the total charge density at $y/l = -6.7$ and $t = 140$ (as indicated by the arrow). The time is normalized by l/u_0.

effect of the finite cyclotron radius in the $x - y$ plane is included. Detailed descriptions on the initial setup for the Vlasov simulation are given in Ref. [42].

Figure 5 shows the the spatial profiles of the ion density N_i and the electric field δE_y component. The plasma void is formed on the nightside of the body while plasma particles accumulate on the dayside surface of the body. At both sides of the plasma void in the nightside, there exist electric fields called "wake" fields. It is found that the structure of the wake field becomes asymmetric, with a strong bipolar signature at the $+y$ side and a weak unipolar signature at the $-y$ side. In the present simulation with the out-of-plane IMF, the trajectory of the $\vec{E} \times \vec{B}$ drift motion of ions becomes a trochoid. In this case, ions with a large gyro radius can penetrate into the wake from the $+y$ side of the wake, where the electric force $\vec{F} = q\vec{E}$ and the density gradient ∇n are in the same direction, i.e., $\nabla n \cdot \vec{F} > 0$. On the other hand, ions with a large gyro radius are absorbed at the surface of the dielectric body and cannot penetrate into the wake from the $-y$ side of the wake where $\nabla n \cdot \vec{F} < 0$. This feature results in the asymmetric structure of the wake fields.

6. Conclusion

In this chapter, numerical schemes of electromagnetic Vlasov simulations for space plasma are briefly reviewed. A latest parallel Vlasov-Maxwell solver with a conservative scheme has successfully applied to magnetic reconnection [31], the K-H instability [32],

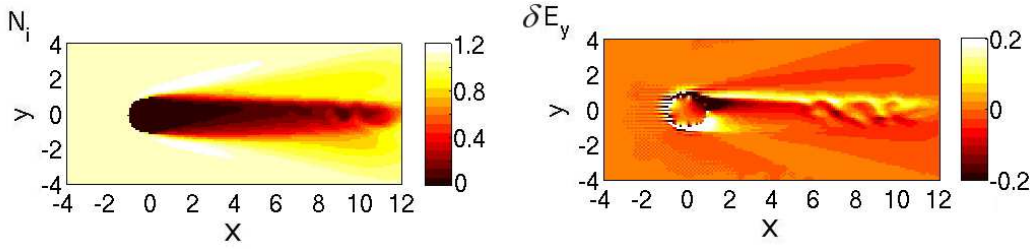

Figure 5. Spatial profiles of the ion density N_i and the electric field δE_y component. The density is normalized by n_0. The electric field is normalized by $|B_0 V_S|$. The distance is normalized by the radius of the object R_S.

and the interaction between solar/stellar winds and dielectric bodies [33]. Currently, 256-1024 cores are used for the parallel computations. However, future Peta-scale supercomputers with 100,000 cores are necessary for 3P3V simulations.

It should be noted, finally, that the numerical schemes for the Vlasov-Maxwell solver is still developing. That is, the numerical schemes presented in this chapter is NOT the final goal of Vlasov-Maxwell solvers; There are still many unsolved issues for the numerical integration of the Vlasov equations in basic numerical problems of multidimensional advection and rotation.

Acknowledgments

This work was supported by MEXT/JSPS under Grant-in-Aid for Young Scientists (B) No.21740352 and No.23740367. The computer simulations were performed on the Hitach HA8000 (T2K) supercomputer system at University of Tokyo and the Fujitsu FX1 and HX600 supercomputer systems at Nagoya University. The computer resources were provided as a computational joint research program at the STEL, Nagoya University, and as a JHPCN program at the Joint Usage/Research Center for Interdisciplinary Large-Scale Information Infrastructures.

The author is grateful to K. Togano, Y. Ito, K. Fukazawa, Y. Nariyuki, Y. Matsumoto, T. K. M. Nakamura, and T. Ogino for discussions.

References

[1] Darwin, C. G. *Philos. Mag.* 1920, 39, 537–551.

[2] Joyce, G.; Knorr, G.; Meier, H. K. *J. Comput. Phys.* 1971, 8, 53–63.

[3] Emery, M. H.; Joyce, G. *J. Comput. Phys.* 1973, 11, 493–506.

[4] Shoucri, M.; Gagne, R. R. J. *J. Comput. Phys.* 1976, 22, 238–242.

[5] Klimas, A. J. *J. Comput. Phys.* 1983, 50, 270–306.

[6] Cheng, C. Z.; Knorr, G. *J. Comput. Phys.* 1976, 22, 330–351.

[7] Gagne, R. R. J.; Shoucri, M.M. *J. Comput. Phys.* 1977, 24, 445–449.

[8] Yanenko, N. N.; Holt, M. *The method of fractional steps: The solution of problems of mathematical physics in several variables*, Springer-Verlag: New York, 1971.

[9] Cheng, C. Z. *J. Comput. Phys.* 1977, 24, 348–360.

[10] Ghizzo, A.; Huot, F.; Bertrand, P. *J. Comput. Phys.* 2003, 186, 47–69.

[11] Sonnendrucker, E.; Roche, J.; Bertrand, P.; Ghizzo, A. *J. Comput. Phys.* 1999, 149, 201–220.

[12] Pohn, E.; Shoucri, M.; Kamelander, G.; *Comput. Phys. Commun.* 2005, 166, 81–93.

[13] Utsumi, T.; Kunugi, T.; Koga, J. *Comput. Phys. Commun.* 1998, 108, 159–179.

[14] Nakamura, T.; Yabe, T. *Comput. Phys. Commun.* 1999, 120, 122–154.

[15] Umeda, T., Y. Omura, P. H. Yoon, R. Gaelzer, and H. Matsumoto, *Phys. Plasmas* 2003, 10, 382–391.

[16] Filbet, F.; Sonnendrucker, E.; Bertrand, P. *J. Comput. Phys.* 2001, 172, 166–187.

[17] Arber, T. D.; Vann, R. G. L. *J. Comput. Phys.* 2002, 180, 339–357.

[18] Elkina, N. V.; Buchner, J. *J. Comput. Phys.* 2005, 213, 862–875.

[19] Umeda, T.; Ashour-Abdalla, M.; Schriver, D. *J. Plasma Phys.* 2006, 72, 1057–1060.

[20] Idomura, Y.; Ida, M.; Tokuda, S.; Villard, L. *J. Comput. Phys.* 2007, 226, 244–262.

[21] Umeda, T. *Earth Planets Space* 2008, 60, 773–779.

[22] Crouseilles, N.; Mehrenberger, M.; Sonnendrucker, N. *J. Comput. Phys.* 2010, 229, 1927–1953.

[23] Filbet, F.; Sonnendrucker, E. *Comput. Phys. Commun.* 2003, 150, 247–266.

[24] Begue, M. L.; Ghizzo, A.; Bertrand, P.; *J. Comput. Phys.* 1999, 151, 458–478.

[25] Grandgirard, V.; Brunetti, M.; Bertrand, P.; Besse, N.; Garbet, X.; Ghendrih, P.; Manfredi, G.; Sarazin, Y.; Sauter, O.; Sonnendrucker, E.; Vaclavik, J.; Villard, L. *J. Comput. Phys.* 2006, 217, 395–423.

[26] Idomura, Y.; Ida, M.; Kano, T.; Aiba, N.; Tokuda, S. *Comput. Phys. Commun.* 2008, 179, 391–403.

[27] Valentini, F.; Veltri, P.; Califano, F.; Mangeney, A. *Phys. Rev. Lett.* 2008, 101, 025006.

[28] Valentini, F.; Veltri, P.; Mangeney, A. *J. Comput. Phys.* 2005, 210, 730–751.

[29] Eliasson B. *J. Comput. Phys.* 2007, 225, 1508–1532.

[30] Schmitz, H.; Grauer, R. *Phys. Plasmas* 2006, 13, 092309.

[31] Umeda, T.; Togano, K.; Ogino, T. *Phys. Plasmas* 2010, 17, 052103.

[32] Umeda, T.; Miwa, J.; Matsumoto, Y.; Nakamura, T. K. M.; Togano, K.; Fukazawa, K.; Shinohara, I. *Phys. Plasmas* 2010, 17, 052311.

[33] Umeda, T.; Kimura, T.; Togano, K.; Fukazawa, K.; Matsumoto, Y.; Miyoshi, T.; Terada, N.; Nakamura, T. K. M.; Ogino, T. *Phys. Plasmas* 2011, 18, 012908.

[34] Umeda, T.; Togano, K.; Ogino, T. *Comput. Phys. Commun.* 2009, 180, 365–374.

[35] Schmitz, H.; Grauer, R. *Comput. Phys. Commun.* 2006, 175, 86–92.

[36] Yee, K. S. *IEEE Trans. Antenn. Propagat.* 1966, AP-14, 302–307.

[37] Umeda, T.; Nariyuki, Y.; Kariya, D. A non-oscillatory and conservative semi-Lagrangian scheme with fourth-degree polynomial, submitted.

[38] Birn, J.; Drake, J. F.; Shay, M. A.; Rogers, B. N.; Denton, R. E.; Hesse, M.; Kuznetsova, M.; Ma, Z. W.; Bhattacharjee, A.; Otto, A.; Pritchett, P. L. *J. Geophys. Res.* 2001, 106, 3715–3719.

[39] Karimabadi, H.; Daughton, W.; Scudder, J. *Geophys. Res. Lett.* 2007, 34, L13104.

[40] Shay, M. A.; Drake, J. F.; Swisdak, M. *Phys. Rev. Lett.* 2007, 99, 155002.

[41] Matsumoto, Y.; Hoshino, M. *J. Geophys. Res.* 2006, 111, A05213.

[42] Umeda, T. Effect of ion cyclotron motion on the structure of wakes: A Vlasov simulation, *Earth Planets Space* 2011, in press.